Rock and Soil Mechanics

Volume 42 | Issue 11 Article 6

2-23-2022

Nonlocal peridynamic method for porous media seepage simulation

Peng-fei MA

Shu-chen LI
shuchenli@sdu.edu.cn

Xiu-wei WANG

Hui-ying ZHOU

See next page for additional authors

Custom Citation

MA Peng-fei, LI Shu-chen, WANG Xiu-wei, ZHOU Hui-ying, WANG Man-ling, ZHAO Yi-min. Nonlocal peridynamic method for porous media seepage simulation[J]. Rock and Soil Mechanics, 2021, 42(11): 3147-3156.

Nonlocal peridynamic method for porous media seepage simulation

Authors

Peng-fei MA, Shu-chen LI, Xiu-wei WANG, Hui-ying ZHOU, Man-ling WANG, and Yi-min ZHAO

Rock and Soil Mechanics 2021 42(11): 3147−3156 ISSN 1000−7598
https: //doi.org/10.16285/j.rsm.2021.5340 rocksoilmech.researchcommons.org/journal

Nonlocal peridynamic method for porous media seepage simulation

MA Peng-fei, LI Shu-chen, WANG Xiu-wei, ZHOU Hui-ying, WANG Man-ling, ZHAO Yi-min
Geotechnical and Structural Engineering Research Center, Shandong University, Jinan, Shandong 250061, China

Abstract: Based on the establishment of peridynamic nonlocal porous media seepage model, several kernel functions reflecting the degree of nonlocal effect are introduced to improve the calculation accuracy, and the peridynamic permeability coefficients corresponding to different kernel functions are derived. In the two-dimensional seepage model, the Weibull-distributed permeability coefficient model and the fracture network seepage model are established to realize the heterogeneous seepage in porous media matrix and fracture, respectively, which make up for the shortage of classical peridynamic model that cannot well simulate the heterogeneous seepage in porous media such as rock and soil. Different kernel function models are tested in simulating one-dimensional seepage problems, and the influence of kernel functions on simulation results is analyzed. The results show that the improved model can well converge to the theoretical solution, and the polynomial kernel function has the highest convergence accuracy relative to other kernel functions. Then, the polynomial kernel function is introduced into the two-dimensional model, and the corresponding two-dimensional permeability coefficient is derived. The proposed heterogeneous seepage model is employed in the simulation of two-dimensional seepage in porous media with and without fracture, and the simulation results show that the proposed model can well simulate the heterogeneous seepage process in rock materials, proposing a wide application prospect in porous media seepage simulation.

Keywords: porous media; peridynamics; nonlocal method; seepage simulation

1 Introduction

Numerous natural pores and structural fractures exist in porous media such as soil and rock, providing the space for groundwater transportation and storage[1–3]. In recent years, with the increase of high slope and underground tunnelling projects, the engineering disasters caused by groundwater have been frequently encountered[4–5], resulting in significant economic loss. The seepage features of groundwater in porous media are hot topics in soil mechanics and rock mechanics[6–9]. The pores and fractures that cannot be quantified in porous media have a great influence on the seepage characteristics, making it very difficult to investigate the seepage problems by theoretical methods. Meanwhile, there are also some limitations in investigating the seepage problems by experimental approaches, such as long cycles, high costs, and difficulty in experimental parameters determination. With the development of computer technology, more and more researchers adopt numerical simulation to investigate the seepage features of porous media.

The continuous medium model based on the flow equivalence principle evenly distributes the permeabilities of pores and fractures in the continuous medium, which is suitable to simulate the seepage in the medium with few macro fractures[10–11]. The fracture network model regards the fluid flow in fractures as pipeline flow, which has some advantages in simulating the fracture seepage[12–13]. By combining the advantages of the above two models, the dual media model is adopted, where the permeabilities of fracture and matrix are simulated with dual meshes, respectively. The pore medium stores water and the fractured medium transports water, which matches the real situation of heterogeneous porous media seepage well[14].

The peridynamic method, which describes the f physical field by integral formulation, can avoid the numerical singularity around the crack tip when employing the differential formulation[15–16], so that has been widely applied in structure failure simulations[17–18]. The diffusion problems such as thermal conduction and seepage that have non-local features can also be described by peridynamics. Gerstle et al.[19] first established the peridynamic model for thermal and electrical conduction and proposed its analytical and numerical solution. Bobaru et al. proposed the non-steady thermal diffusion equation based on Fourier's law and energy conservation law and studied the thermal conduction of fractured medium[20]. Wang et al.[21] proposed the conventional peridynamic thermal diffusion equation by employing the Euler equation in the Lagrange coordinate system. Liu et al. [22] investigated the temperature field variation in functional gradient material under thermal load using the peridynamic model. For the porous media seepage problems, Jabakhanji et al.[23] proposed a peridynamic model for moisture diffusion in homogenous unsaturated soil and determined the humidity flux expression formulation and the relationship between hydraulic conductivity and the traditional Darcy's permeability. Based on the classical Biot's pore pressure theory, Zhou et al.[24] established the fractured rock mass seepage model and hydraulic fracturing model based on the classic Biot pore theory

Received: 13 May 2021 Revised: 18 August 2021
This work was supported by the National Natural Science Foundation of China (Grant Nos.51879150 and 41831278).
First author: MA Peng-fei, male, born in 1994, PhD candidate, majoring in numerical simulation of geotechnical engineering. E-mail: mapengfeisdu@163.com
Corresponding author: LI Shu-chen, male, born in 1973, PhD, Professor, research interests: numerical simulation of geotechnical engineering. E-mail: shuchenli@sdu.edu.cn

using the peridynamics method.

In the peridynamic diffusion theory, the physical quantities at the discrete points interact with each other within a certain distance and no longer interact if they exceed the critical value. In nonlocal theory, the interaction becomes weaker with the increase of distance between two material points, and the calculation accuracy will be affected if the relationship between interaction degree and distance is not considered. In addition, the micro-fractures that cannot be quantified will lead to the heterogeneity of porous media such as soil and rock, and the non-uniform diffusion cannot be well reflected by the homogeneous method.

Based on the existing research work, the peridynamic diffusion equation for porous media seepage is established in the present paper, where, the kernel functions that reflect the nonlocal effect are introduced to improve the calculation accuracy. The permeability coefficients corresponding to different kernel functions are derived, and the heterogeneous seepage model for porous media is established based on the Weibull distribution theory and the fracture network model. The established model is employed to simulate the porous media seepage process, and the simulation results are compared with theoretical solutions to verify the effectiveness of the proposed method. Meanwhile, the seepage processes in heterogeneous matrix and fracture are simulated, and the results show that the proposed method is feasible for porous media seepage simulation.

2 Seepage equation

2.1 Basic equations

As shown in Fig. 1, the porous medium domain is discretized into material points where water is assumed to be stored. The volume of material point x is $\mathrm{d}V_x$, and the water head at this point is $H(x)$. The moisture exchange occurs between adjacent material points within an influence radius of δ. For example, material point x' is the interaction point of material point x, and they are connected with the bond xx' where water can be transported. The transported water in unit time and unit water head difference can be represented by the peridynamic hydraulic conductivity density $C(x,x')$, which can be derived from the peridynamic permeability coefficient $k(x,x')$ [23]

$$C(x,x')=\frac{k(x,x')}{|xx'|} \tag{1}$$

If there is a water head difference between material points x and x', the water content increments at both ends of the bond xx' can be calculated by[23]

$$\Delta V_{\mathrm{m}}(x,x')=k(x,x')\frac{[H(x')-H(x)]}{|xx'|}\mathrm{d}V_x\mathrm{d}V_{x'} \tag{2}$$

$$\Delta V_{\mathrm{m}}(x',x)=k(x',x)\frac{[H(x)-H(x')]}{|x'x|}\mathrm{d}V_{x'}\mathrm{d}V_x \tag{3}$$

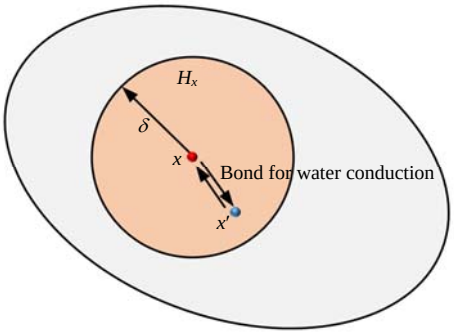

Fig. 1 Interaction between material points

where $\Delta V_{\mathrm{m}}(x,x')$ and $\Delta V_{\mathrm{m}}(x',x)$ denote the water content increments at material points x and x', respectively. Since the bond xx' cannot store water, the water content increments at both ends meet $\Delta V_{\mathrm{m}}(x,x')=-\Delta V_{\mathrm{m}}(x',x)$. $k(x',x)$ is the peridynamic permeability coefficient. According to Eqs. (2) and (3), $k(x,x')=k(x',x)$, which indicates that the permeability coefficients along the opposite directions of one bond are the same.

Since the nonlocal property of peridynamics, the change of the moisture content at material point x should be equal to the total diffusion of other material points in the neighborhood domain H_x, considering the external source $S(x)$ [23]

$$\frac{\partial\theta(x)}{\partial t}=\int_{H_x}k(x,x')\frac{[H(x')-H(x)]}{|xx'|}\mathrm{d}V_{x'}+S(x) \tag{4}$$

where t is the time; $\theta(x)$ indicates the volume of water stored at material point x. By integrating Eq. (4) within the domain R, the moisture content change in the domain can be obtained[23]:

$$\int_{H_x}\frac{\partial\theta(x)}{\partial t}\mathrm{d}V_x=\int_{H_x}\int_{H_x}k(x,x')\frac{[H(x')-H(x)]}{|xx'|}\cdot \mathrm{d}V_{x'}\mathrm{d}V_x+\int_{H_x}S(x)\mathrm{d}V_x \tag{5}$$

The first integral term on the right side of the equation can be rewritten as[23]

$$\int_{H_x}\int_{H_x}\frac{k(x,x')H(x')}{|xx'|}\mathrm{d}V_{x'}\mathrm{d}V_x-\int_{H_x}\int_{H_x}\frac{k(x,x')H(x)}{|xx'|}\mathrm{d}V_{x'}\mathrm{d}V_x \tag{6}$$

Performing the variable substitution for the second term in formula (6), the results of formula (6) are 0 as the equal permeability coefficients. Thus, Eq. (5) can be simplified as

$$\int_{H_x}\frac{\partial\theta(x)}{\partial t}\mathrm{d}V_x=\int_{H_x}S(x)\mathrm{d}V_x \tag{7}$$

Equation (7) indicates that the change of total moisture content within the interaction region of material point x is only related to the external term and the total moisture in the region remains unchanged.

2.2 Nonlocal permeability coefficient

According to the nonlocal theory, the relationship between interaction effect and distance has a great influence on the calculation result. In order to improve the calculation accuracy and stability, Huang et al.[25] introduced the kernel function that describes the interaction between material points into the mechanic model. In this section, based on the previous studies, different kernel functions are introduced into the nonlocal diffusion model and the corresponding permeability coefficients are calculated.

The relationship between peridynamic permeability coefficient $k(x,x')$ and traditional Darcy's permeability coefficient K is usually determined by assuming the amount of water flowing through the unit section area is the same. Incorporating the kernel function, the following equation is obtained

$$k(x,x')=k(\xi)=k(0,\delta)g(\xi,\delta) \tag{8}$$

where ξ is the relative position; δ is the radius of neighborhood domain; and $g(\xi,\delta)$ is the correction term with respect to the nonlocal feature, which meets

$$\left.\begin{aligned} &g(\xi,\delta)=g(-\xi,\delta)\\ &\lim_{\xi\to 0}g(\xi,\delta)=\max g\\ &\lim_{\xi\to\delta}g(\xi,\delta)=0\\ &\int_{-\infty}^{\infty}\lim_{\xi\to 0}g(\xi,\delta)=\int_{-\infty}^{\infty}\Delta(\xi)\mathrm{d}x=1 \end{aligned}\right\} \tag{9}$$

where $\Delta(\xi)$ is the Dirac Delta function, and the proposed seepage model will degenerate to the classic seepage model if $g(\xi,\delta)$ =1. Herein, taking the one-dimensional seepage model as an example, the expressions of permeability coefficients corresponding to the linear type g_1, quadratic type g_2, polynomial type g_3 , and cosine type g_4 are derived.

The seepage model is shown in Fig. 2. The water flows to the right side from the left side with a higher water head through material point *x* and section *S*. The left and right sets (H_x^{l} and H_x^{r}) of the neighborhood domain (H_x) of material point *x* can be defined as

$$H_x^{\mathrm{l}}=\left\{x_{\mathrm{l}}\in H_x\middle|xx_{\mathrm{l}}\cdot S_{\perp}>0\right\} \tag{10}$$

$$H_x^{\mathrm{r}}=\left\{x_{\mathrm{r}}\in H_x\middle|x_{\mathrm{r}}\notin H_x^{\mathrm{l}}\right\} \tag{11}$$

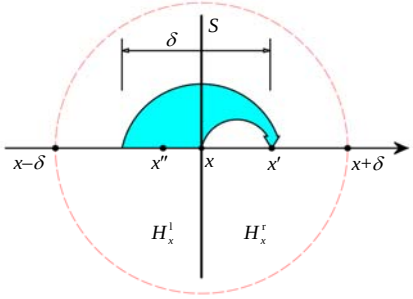

Fig. 2 One-dimensional seepage model[26]

where, x_{l} and x_{r} are the material points located at the left and right sides of material point *x*; xx_{l} is the line segment between the two material points; and $S_{\perp}$ indicates the perpendicular plane at material point *x*.

The moisture exchange occurs between the material point x_{l} in H_x^{l} and other surrounding material points. Considering water flows through section *S* from H_x^{l}, the material points in H_x^{r}, where the moisture exchange, can be denoted as

$$H_{x_{\mathrm{r}}}^{\mathrm{l}}=\left\{x'_{\mathrm{r}}\in H_x^{\mathrm{r}}\middle|x_{\mathrm{l}}x'_{\mathrm{r}}\middle|\leqslant\delta,x_{\mathrm{l}}\in H_x^{\mathrm{l}}\right\} \tag{12}$$

As shown in Fig.2, the coordinates of the material points at $H_{x_{\mathrm{r}}}^{\mathrm{l}}$ and H_x^{l} are x' and x'', respectively. Combining Eq. (5), the total amount of water flux ($q(x)$) flowing through section *S* at a certain moment can be calculated by[26]

$$q(x)=-\int_{H_x^{\mathrm{l}}}\int_{H_{x_{\mathrm{r}}}^{\mathrm{l}}}k(x'',x')\frac{\left[H(x')-H(x'')\right]}{\left|x''x'\right|}\mathrm{d}V_{x'}\mathrm{d}V_{x''} \tag{13}$$

Eq. (13) can be further written as

$$q(x)=-\int_{x-\delta}^{x}\int_{x}^{x''+\delta}k(x'',x')\frac{\left[H(x')-H(x'')\right]}{\left|x''x'\right|}\mathrm{d}x'\mathrm{d}x'' \tag{14}$$

According to classic Darcy's law, the total amount of water flowing through section *S* is obtained by

$$q(x)=K\frac{\partial H(x)}{\partial x} \tag{15}$$

Assuming that the hydraulic gradient is linearly distributed in the model, namely $H(x)=ax+c$, where a and c are both constants. Eq. (15) can be rewritten as

$$q(x)=-Ka \tag{16}$$

Due to the linear hydraulic gradient a , Eq. (14) can be rewritten as

$$q(x)=-\int_{x-\delta}^{x}\int_{x}^{x''+\delta}k(x'',x')a\mathrm{d}x'\mathrm{d}x'' \tag{17}$$

When the kernel function is g_1, $k(x'',x')$ can be formulated as the constant $k(0,\delta)$ multiplied by a linear function $1-\xi/\delta$. Substituting $k(x'',x')$ into Eq. (17) yields

$$\begin{aligned} q(x)=&-\int_{x-\delta}^{x}\int_{x}^{x''+\delta}k(0,\delta)\left(1-\frac{\xi}{\delta}\right)a\mathrm{d}x'\mathrm{d}x''=\\ &-\int_{x-\delta}^{x}\int_{x}^{x''+\delta}k(0,\delta)\left(1-\frac{x'-x''}{\delta}\right)a\mathrm{d}x'\mathrm{d}x''=\\ &-\int_{x-\delta}^{x}k(0,\delta)a\left(x''+\frac{x''^2}{2\delta}+\frac{\delta}{2}\right)\mathrm{d}x''=-\frac{k(0,\delta)a\delta^2}{6} \end{aligned} \tag{18}$$

Since Eq. (16) is equal to Eq. (18), $k(0,\delta)$ has the form as

$$k(0,\delta)=\frac{6K}{\delta^2} \tag{19}$$

If taking the quadratic type g_2, Eq. (17) can be

rewritten as

$$q(x)=-\int_{x-\delta}^{x}\int_{x}^{x''+\delta}k(0,\delta)\left(1-\left(\frac{\xi}{\delta}\right)^2\right)a\mathrm{d}x'\mathrm{d}x''=$$

$$-\int_{x-\delta}^{x}k(0,\delta)a\frac{(\delta+x'')^2(2\delta-x'')}{3\delta^2}\mathrm{d}x''=-\frac{k(0,\delta)a\delta^2}{4} \tag{20}$$

Since Eq. (16) is equal to Eq. (20), $k(0,\delta)$ has the form as

$$k(0,\delta)=\frac{4K}{\delta^2} \tag{21}$$

Similar operations can be performed for the remaining two types of kernel functions, and the results are listed in Table 1.

Table 1 Kernel functions and corresponding modulus

Kernel functions	g_1	g_2	g_3	g_4
$g(\xi,\delta)$	$1-\frac{\xi}{\delta}$	$1-\left(\frac{\xi}{\delta}\right)^2$	$\left(1-\left(\frac{\xi}{\delta}\right)^2\right)^2$	$\cos\left(\frac{\pi\xi}{2\delta}\right)$
$k(0,\delta)$	$\frac{6K}{\delta^2}$	$\frac{4K}{\delta^2}$	$\frac{6K}{\delta^2}$	$\frac{\pi^2K}{2(\pi-2)\delta^2}$

In this section, the permeability coefficients corresponding to different kernel functions are derived, and the influence of different kernel functions on the calculation result will be discussed in section 3.

2.3 Heterogeneous seepage

The pores and fractures that cannot be quantified in the porous media make the heterogeneous behavior of the matrix. In this section, the Weibull-distributed matrix permeability coefficient and the fracture network seepage model are introduced to simulate the heterogeneous seepage in porous media.

As shown in Fig. 3, the angle between the horizontal axis and the perpendicular direction ($S_\perp$) of the section S at material point x is φ. the corresponding material points, have moisture exchange, at each side of material point x can be denoted as $x'(r',\theta)$ and $x''(r'',\theta+\pi)$ in the polar form, respectively, where x' and x'' have the same meaning as the last section and are coplanar with material point x. The total amount of water flowing along the direction of $S_\perp$ can be obtained by[26]

$$q(\varphi)=\int_{\varphi-\frac{\pi}{2}}^{\varphi+\frac{\pi}{2}}\int_{\delta}^{0}\int_{0}^{\delta-r''}k(x',x'')\left[H(x'')-H(x')\right]\cdot \cos(\theta-\varphi)\mathrm{d}r'\mathrm{d}r''\mathrm{d}\theta \tag{22}$$

Assuming that the hydraulic gradient distribution in the model is $H(x)=ax\cdot\hat{j}+c$, where the water head difference at $\hat{j}=(1,0)$ can be denoted as

$$H(x'')-H(x')=a(r'+r'')\sin\theta \tag{23}$$

Taking the kernel function $g(\xi,\delta)=1$ of the permeability coefficient is $k(x',x'')$ as an example, Eq. (22) is substituted into Eq. (23)

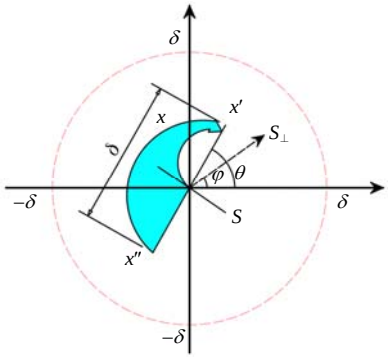

Fig. 3 Two-dimensional seepage model[26]

$$q(\varphi)=\int_{\varphi-\frac{\pi}{2}}^{\varphi+\frac{\pi}{2}}\int_{\delta}^{0}\int_{0}^{\delta-r''}ka(r'+r'')\sin\theta\cos(\theta-\varphi)\mathrm{d}r'\mathrm{d}r''\mathrm{d}\theta \tag{24}$$

Equation (24) can be further integrated as

$$q(\varphi)=-\frac{1}{6}ka\pi\delta^3\sin\varphi \tag{25}$$

The water flow calculated by Darcy's law is

$$q(\varphi)=-Ka\sin\varphi \tag{26}$$

Combining Eq. (29) and Eq. (30) yields

$$k=\frac{6K}{\pi\delta^3} \tag{27}$$

The permeability coefficients corresponding to the remaining kernel functions can be obtained with similar operations. Due to the different permeability of microcracks in the porous media, the Weibull-distributed permeability coefficient is introduced to describe the heterogeneous property of porous media

$$f(u)=\frac{m}{u_0}\left(\frac{u}{u_0}\right)^{m-1}\exp\left[-\left(\frac{u}{u_0}\right)^m\right] \tag{28}$$

where u is the scale parameter at material points (e.g., permeability coefficient); u_0 is the average value of u; m is the shape parameter employed in the distribution function, and the probability functions with different m are shown in Fig. 4. The smaller the m is, the more uneven distribution of material point parameters will be. In the present paper, the permeability coefficient (K_i) of the porous medium is employed for u. According

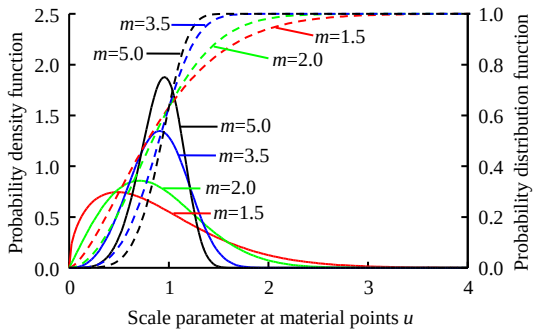

Fig. 4 Probability functions corresponding to different shape parameters

to Eq. (27), the peridynamic permeability coefficient k_i at material point x is obtained, and the mean value is used for moisture exchange calculation between two material points.

As shown in Fig. 5, the interaction region is separated by a macro fracture, and the interaction forces of the broken bonds are equal to 0 (the dashed lines in Fig. 5). In this paper, a similar approach is employed in the seepage model, where the bonds separated by the macro-fracture are indicated as a fracture network with a much larger permeability coefficient than that of the matrix. Therefore, the seepage in fractures can be simulated. The permeability coefficient of fracture (K_f) can be determined with classic Darcy's law, and the cubic law is employed to determine the permeability coefficient at low Reynolds numbers, namely

$$K_f = \frac{w^2}{12\mu} \tag{29}$$

where w is the fracture aperture and μ is the water viscosity. The peridynamic permeability coefficient k_f can be then determined with Eq. (24).

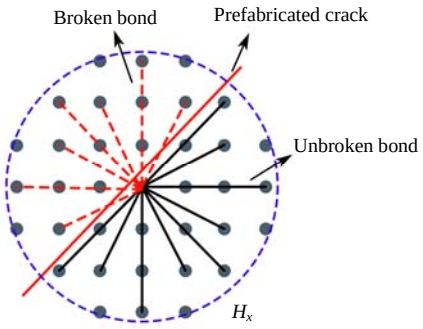

Fig. 5 Regions separated by fracture

3 One-dimensional seepage simulation

3.1 Numerical simulation scheme

To verify the feasibility of the proposed model and investigate the influence of different kernel functions on the simulation results, a one-dimensional seepage simulation is taken as an example. As shown in Fig. 6, the length (L) and width (H) of the rock are 1.0 m and 0.4 m, respectively. The permeability coefficient along the horizontal direction is K, and the upper and bottom surfaces of the rock are impermeable layers. Continuous water pressures P_L and P_R ($P_L > P_R$) are applied on the left and right sides of the rock, respectively. The initial pore water pressure of the medium is set as 0, thus water will flow toward the right side from the left side.

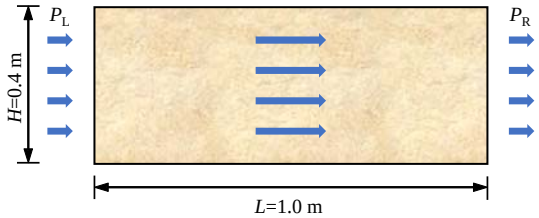

Fig. 6 One-dimensional steady-state seepage

This model is discretized into 200×80 computation nodes, with the nodal distance $\Delta x = 0.005$ m and the interaction radius $\delta = 3.015\Delta x$. The permeability coefficient along the horizontal direction is $K = 0.048\ 5$ m/d, and the time step dt is 0.001 d. The water pressures applied on the left and right sides of the model are 55 kPa and 15 kPa, respectively.

The analytical solution of the water pressure distribution along the horizontal direction is

$$P(x) = P_L - (P_R - P_L)\frac{x}{L} \tag{30}$$

3.2 Seepage process simulation

The linear model is employed, and the total time step is set as 6 000. The distributions of water pressure along the horizontal direction at different times are shown in Fig. 7.

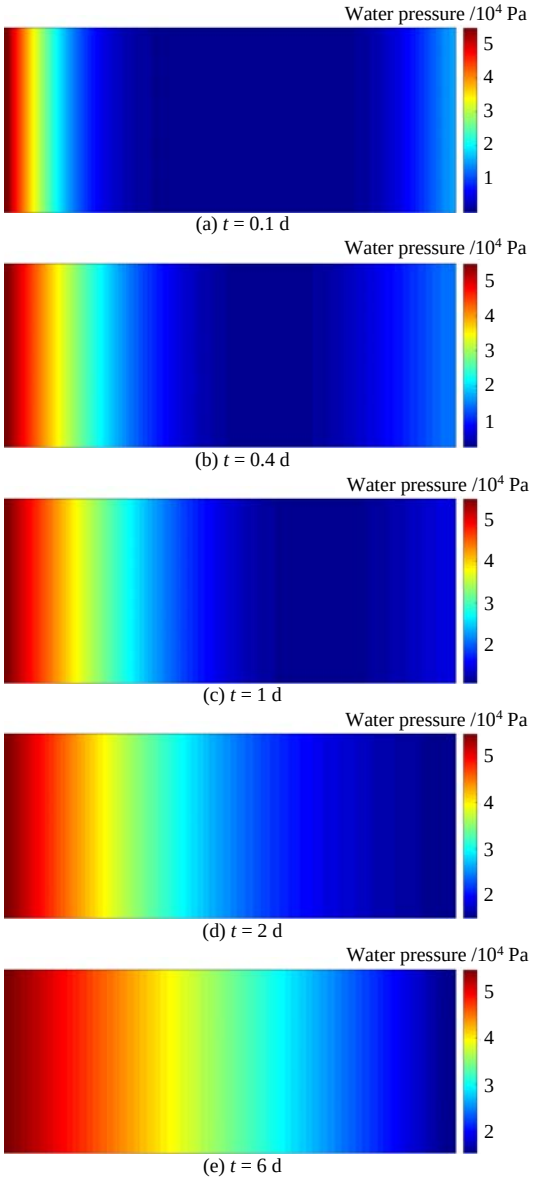

Fig. 7 Water pressure distribution along the horizontal direction

According to the water pressure distribution at different times, it is observed that water driven by the water head differences at both sides flows toward the

middle of the model simultaneously at the initial stage, and the seepage area at the left side is larger than that at the right side at the same moment. As time increases, the water from both sides meets at the middle of the model, and flow from left to right due to the higher water head at the left side. The simulated seepage features are in coincide with the real seepage process, validating the feasibility of the proposed method.

The comparison between the simulated water pressures and the analytical solution at different times is shown in Fig. 8. Since the larger horizontal pressure difference, the seepage process develops rapidly at the initial stage. As time increases, the horizontal pressure difference gradually decreases, which in turn affects the seepage process and eventually the simulated water pressure distribution converges to the analytical solution. Therefore, the feasibility of the proposed peridynamic model is further validated.

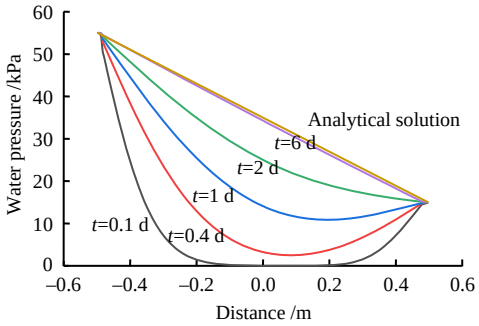

Fig. 8 Comparison of water pressure distributions between simulated results and analytical solution

3.3 Kernel function optimization

The kernel functions have a great influence on the calculation accuracy. Based on the analysis of linear kernel function g_1, the seepage processes corresponding to the kernel functions of quadratic type g_2, polynomial type g_3, and cosine type g_4 can be simulated in the same way, and the results are shown in Fig. 9.

In Fig. 9, the calculation accuracy of the kernel function of polynomial type g_3 is better than that of other kernel functions. The convergence accuracy of the four kernel functions in order is polynomial type g_3, linear type g_1, cosine type g_4 and quadratic type g_2. Overall, the polynomial kernel function is employed in subsequent simulations.

4 Heterogeneous seepage simulation

4.1 Nonlocal two-dimensional seepage model

To improve the calculation accuracy, the kernel function of polynomial type g_3 is introduced into Eq. (28), and the corresponding permeability coefficient k can be written as

$$k = k(0,\delta)\left(1-\left(\frac{\xi}{\delta}\right)^2\right)^2 \tag{31}$$

Substituting Eq. (31) into Eq. (24), the following equation can be obtained after integration

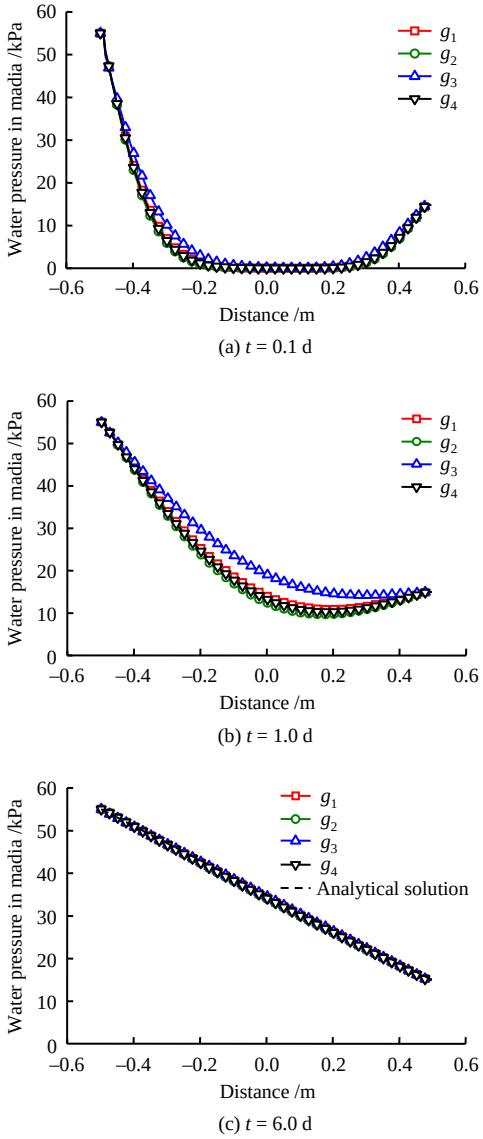

Fig. 9 Influence of kernel functions on simulation results

$$q(\varphi) = -\frac{4}{105}k(0,\delta)a\pi\delta^3\sin\varphi \tag{32}$$

Since Eq. (32) is equivalent to Eq. (25), $k(0,\delta)$ can be written as

$$k(0,\delta) = \frac{105K}{4\pi\delta^3} \tag{33}$$

In order to verify the feasibility of the proposed model, the classic five-point wells network seepage problem is employed, and the specific model and theoretical solution can be referred to reference [28]. As shown in Fig. 10, the geometry of the seepage model is $L\times H = 1$ m $\times 1$ m, and the permeability coefficient is K. Constant water pressures P_L and P_R are applied at the lower-left corner and upper-right corner of the model, respectively. The initial medium pore water pressure is set to 0, and the surrounding walls of the model are impermeable. With the passage of time, the water seepage from the lower-left corner to the upper right corner.

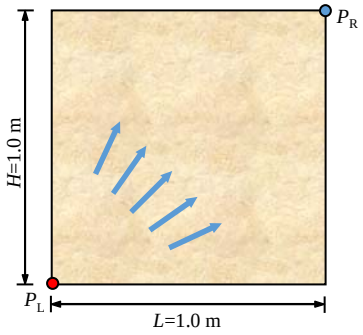

Fig. 10 Two-dimensional seepage problem

The model is discretized into 200×200 computation nodes, and the nodal distance and interaction radius are the same as those in the last section. The permeability coefficient is $K = 0.047\ 5$ m/d , and the water pressures applied on the lower-left corner and upper–right corner are $P_L = 90$ kPa and $P_R = -90$ kPa，respectively. The time step size is $dt = 0.001$ d . The water pressure distributions at different times are shown in Fig. 11, and the comparison between the simulated water pressure distributed on the diagonal line $y = x$ and the analytical solution is shown in Fig. 12.

Figure 11 shows that water gradually seepage in the porous medium from the lower-left corner to the upper right corner driven by the water pressures applied on the corners. With the passage of time, the water pressure distribution gradually converges to the analytical solution, which validates the feasibility of the proposed model.

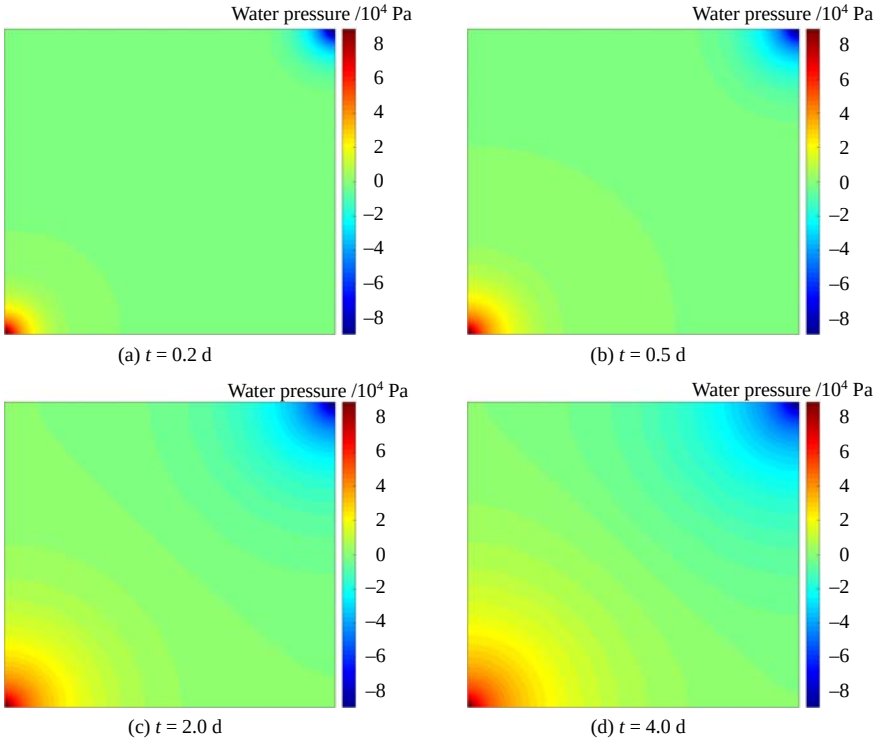

Fig. 11 Distribution of seepage water pressure

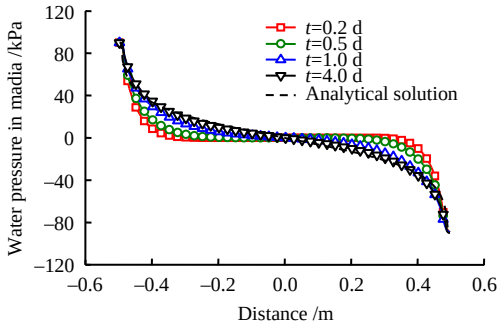

Fig. 12 Comparison of water pressure distributions on diagonal ($y = x$) between simulated results and theoretical solution

4.2 Inhomogeneous seepage in rock matrix

Unquantified micro-fractures in the porous media lead to heterogeneous diffusion, which can be described by the Weibull-distributed permeability coefficient. The material point parameter u is set as the permeability coefficient (K) of the porous medium, and the distribution function is shown as Eq. (34). In addition, the probability distribution curves of the permeability coefficient with respect to different shape parameters (m=1, 2, and 5) are shown in Fig. 13. The distribution of permeability coefficient when m=5 is shown in Fig. 14, where the heterogeneity of the matrix is clearly presented.

$$f(K) = \frac{m}{K_0}\left(\frac{K}{K_0}\right)^{m-1} \exp\left[-\left(\frac{K}{K_0}\right)^{m}\right] \tag{34}$$

The geometry model is selected from the lower-left part ($L \times H = 0.5$ m $\times 0.5$ m) of the model in section 4.1, and a continuous water pressure $P = 90$ kPa is applied at the lower left corner of the model. Taking m=1 as an example, the simulation results are shown in Fig. 15.

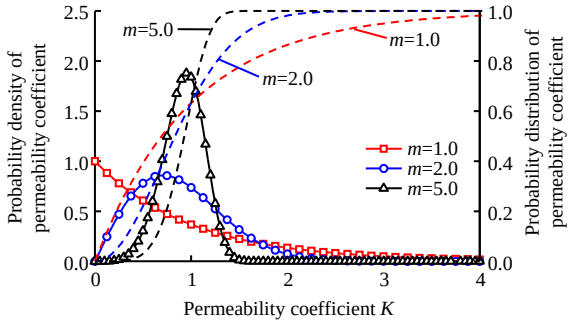

Fig. 13 Probability distribution curves of permeability coefficient

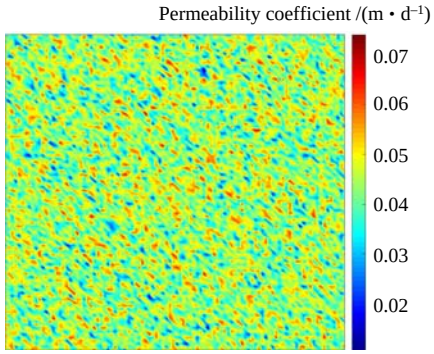

Fig. 14 Weibull-distributed permeability coefficient (*m*=5)

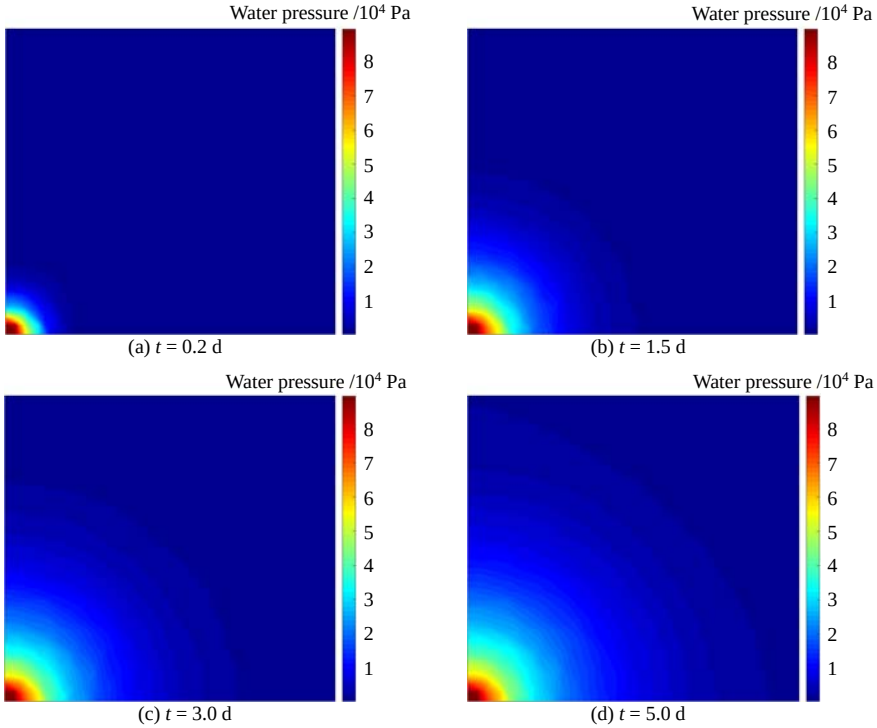

Fig. 15 Inhomogeneous diffusion process

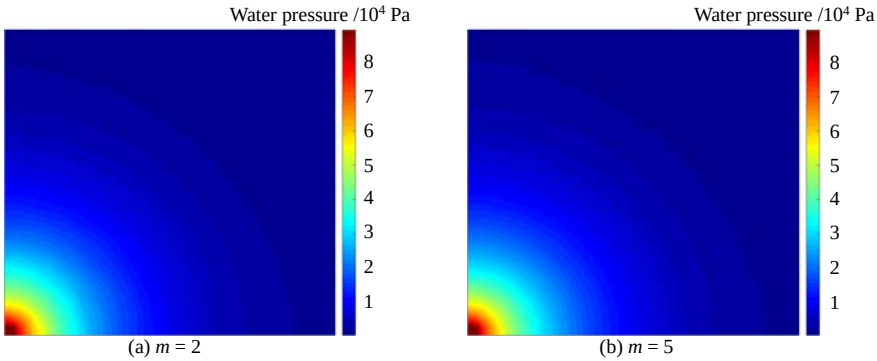

Fig. 16 Calculation results corresponding to different shape parameters

4.3 Inhomogeneous seepage in fracture

The permeability of macro fracture is different from the matrix. In the peridynamics, the bonds separated by fracture can be defined as the fracture region with a much larger permeability coefficient, while the permeability of intact bonds remains the same as the matrix. To verify the seepage process in fractures, the rock mass containing cross fractures shown in Fig. 17 is employed. The model size and nodal distance are the same as those in section 4.1, and the fracture permeability coefficient is $K = 0.057\ 3$ m/s. Since we mainly focus on the water flow in fractures in this section, the permeability coefficient of the matrix is set to 0. The water pressure of 80 kPa is applied on both sides of the model, and the water pressure evolution is shown in Fig. 18.

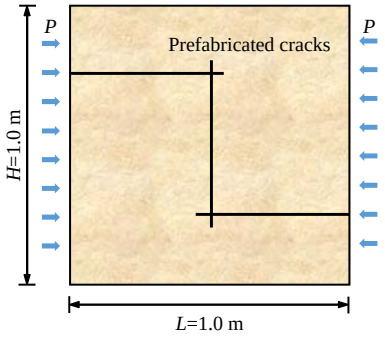

Fig. 17 Fracture seepage model

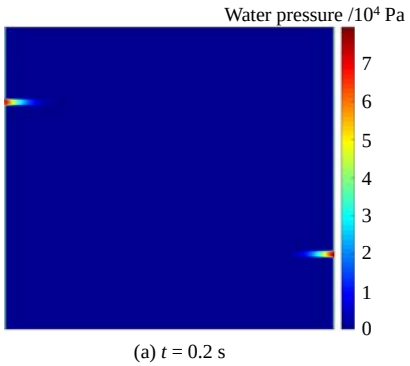

(a) t = 0.2 s

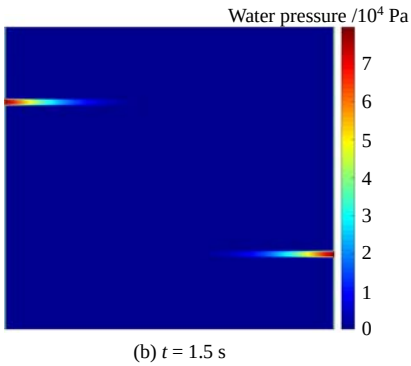

(b) t = 1.5 s

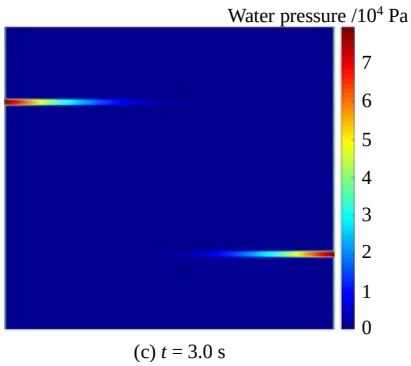

(c) t = 3.0 s

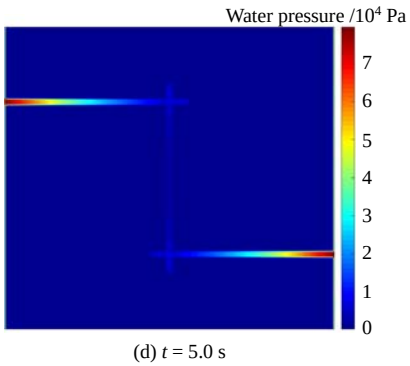

(d) t = 5.0 s

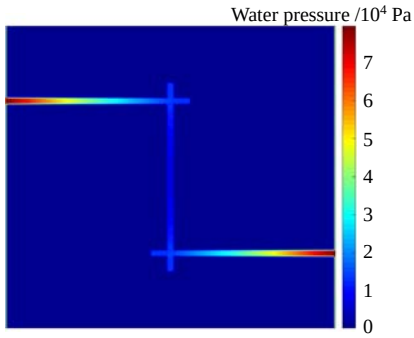

(e) t = 8.0 s

Fig. 18 Seepage process of cross fractures

In Fig. 18, the peridynamic method can well simulate the fracture seepage process. At the initial stage of seepage, water gradually flows into the fracture region from the boundary. With the passage of time, water gradually flows along the fractures and finally meets at the middle of the model, which matches reality well.

5 Conclusion

(1) The peridynamic method is suitable for the porous media seepage simulation, and the governing equations established by integral forms have a good application prospect in the seepage simulation.

(2) The calculation accuracy of the polynomial kernel function is better than that of other kernel functions. The simulated results of the benchmark problems converge to the analytical solutions, which validates the feasibility of the proposed method.

(3) The Weibull-distributed permeability coefficient is suitable for the heterogeneous seepage simulation, and the seepage in fractures can be well simulated with the fracture network seepage model.

References

[1] CHERTKOV VY. Modelling cracking stages of saturated soils as they dry and shrink[J]. European Journal of Soil Science, 2002, 53(1): 105–118.

[2] GRECO R. Preferential flow in macroporous swelling soil with internal catchment: model development and applications[J]. Journal of Hydrology, 2002, 269(3–4): 150–168.

[3] JARVIS N. A review of non-equilibrium water flow and solute transport in soil macropores: principles, controlling factors and consequences for water quality[J]. European Journal of Soil Science, 2010, 58(3): 523–546.

[4] SHE Shi-gang, LIN Peng. Some developments and challenging issues in rock engineering field in China[J]. Chinese Journal of Rock Mechanics and Engineering, 2014, 33(3): 433–457.

[5] CHEN Y F, HONG J M, ZHENG H K, et al. Evaluation of groundwater leakage into a drainage tunnel in Jinping-I

arch dam foundation in Southwestern China: a case study[J]. Rock Mechanics and Rock Engineering, 2016, 49(3): 961–979.

[6] GREVE A, ANDERSEN M, ACWOR R. Investigations of soil cracking and preferential flow in a weighing lysimeter filled with cracking clay soil[J]. Journal of Hydrology, 2010, 393(1–2): 105–113.

[7] YAO Chi, SHAO Yu-long, YANG Jian-hua. Effect of nonlinear seepage on flow and heat transfer process of fractured rocks[J]. Chinese Journal of Geotechnical Engineering, 2020, 42(6): 68–76.

[8] CUI Wei, ZOU Xu, LI Zheng, et al. Experimental study on seepage diffusion movement in fractal rock fractures[J]. Rock and Soil Mechanics, 2020, 41(11): 3553–3562.

[9] LI Bo, HUANG Jia-lun, ZHONG Zhen, et al. Numerical simulation on hydraulic and solute transport properties of 3D crossed fractures[J]. Rock and Soil Mechanics, 2019, 40(9): 3670–3678.

[10] LONG J C, REMER J S, WILSON C R, et al. Porous media equivalents for networks of discontinuous fractures[J]. Water Resources Research, 1982, 18(3): 645–658.

[11] NEUMAN S P. Trends, prospects and challenges in quantifying flow and transport through fractured rocks[J]. Hydrogeology Journal, 2005, 13(1): 124–147.

[12] REICHENBERGER V, JAKOBS H, BASTIAN P, et al. A mixed-dimensional finite volume method for two-phase flow in fractured porous media[J]. Advances in Water Resources, 2006, 29(7): 1020–1036.

[13] YAN X, HUANG Z, YAO J, et al. An efficient embedded discrete fracture model based on mimetic finite difference method[J]. Journal of Petroleum Science and Engineering, 2016, 145:11–21.

[14] KARIMI F M, GONG B, DURLOFSKY L J. Generation of coarse-scale continuum flow models from detailed fracture characterizations[J]. Water Resources Research, 2006, 42(10): 1–9.

[15] SILLING S A. Reformulation of elasticity theory for discontinuities and long-range forces[J]. Journal of Mechanics Physics of Solids, 2000, 48(1): 175–209.

[16] SILLING S A, ASKARI E. A meshfree method based on the peridynamic model of solid mechanics[J]. Computers and Structures, 2005, 83(17): 1526–1535.

[17] ZHU Qi-zhi, NI Tao, ZHAO Lun-yang, et al. Simulations of crack propagation in rock-like materials using peridynamic method[J]. Chinese Journal of Rock Mechanics and Engineering, 2016(Suppl.2), 35: 3507–3515.

[18] WANG Chao, XIONG Wei-peng, YE Li-yu, et al. Analysis of shadowing effect during propeller-ice contact process[J]. Journal of Huazhong University of Science and Technology (Natural Science Edition), 2018, 46(6): 105–110.

[19] GERSTLE W, SILLING S, READ D, et al. Peridynamic simulation of electromigration[J]. Computers Materials and Continua, 2008, 8(2): 75–92.

[20] BOBARU F, DUANGPANYA M. The peridynamic formulation for transient heat conduction[J]. International Journal of Heat and Mass Transfer, 2010, 53(19-20): 4047–4059.

[21] WANG Cai-yun, JIANG Dong-ju, HUANG Dan. Coupled thermo-mechanical deformation and failure analysis based on state-based peridynamics[J]. Chinese Journal of Applied Mechanics, 2020, 37(3): 24–30.

[22] LIU Ying-kai, CHENG Zhan-qi. Transient heat conduction model for functionally graded materials based on peridynamics[J]. Chinese Quarterly of Mechanics, 2018, 39(1): 82–89.

[23] JABAKHANJI R, MOHTAR R H. A peridynamic model of flow in porous media[J]. Advances in Water Resources, 2015, 78: 22–35.

[24] ZHOU X P, WANG Y T, SHOU Y D. Hydromechanical bond-based peridynamic model for pressurized and fluid-driven fracturing processes in fissured porous rocks[J]. International Journal of Rock Mechanics and Mining Sciences, 2020, 132: 104383.

[25] HUANG D, LU G, WANG C. An extended peridynamic approach for deformation and fracture analysis[J]. Engineering Fracture Mechanics, 2015, 141: 196–211.

[26] SHOU Yun-dong. Peridynamic numerical simulation of thermo-hydro-mechanical coupled problems in crack rock[D]. Chongqing: Chongqing University, 2017.

[27] ZIMMERMAN R W, YEO I W. Fluid flow in rock fractures: from the Navier-Stokes equations to the cubic law[J]. Dynamics of Fluids in Fractured Rock, 2000, 122: 213–224.

[28] KATIYAR A, FOSTER J T, OUCHI H. A peridynamic formulation of pressure driven convective fluid transport in porous media[J]. Journal of Computational Physics, 2014, 261: 209–229.